Supplementary material to the publication Koděra et al. (2022): Ferrous hydroxychlorides hibbingite (γ-$Fe_2(OH)_3Cl$) and parahibbingite (β-$Fe_2(OH)_3Cl$) as a concealed sink of Cl and H_2O in ultrabasic and granitic systems

Appendix 1: Simplified geological setting of the Karee platinum mine, located in the southwestern part of the Bushweld Igneus Complex. The mine is based on the UG2 chromitite layer below the adjacent Merensky Reef in the Critical Zone of the Rustenburg Layered Suite (modified from Cawthorn et al. 2009, Kawohl and Frimmel 2016).

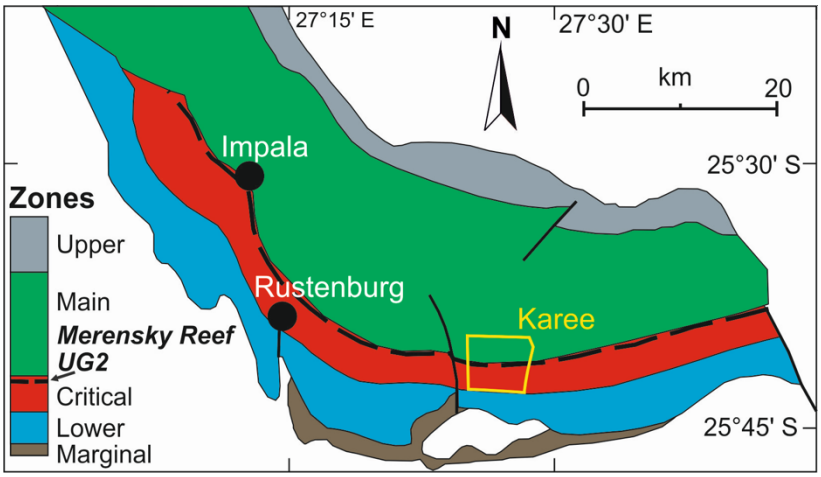

Appendix 2: Geological setting of the Biely Vrch porphyry gold deposit in the schematic structure of the Javorie stratovolcano, hosted by the Central Slovak Volcanic Field (modified from Lexa et al. 1999).

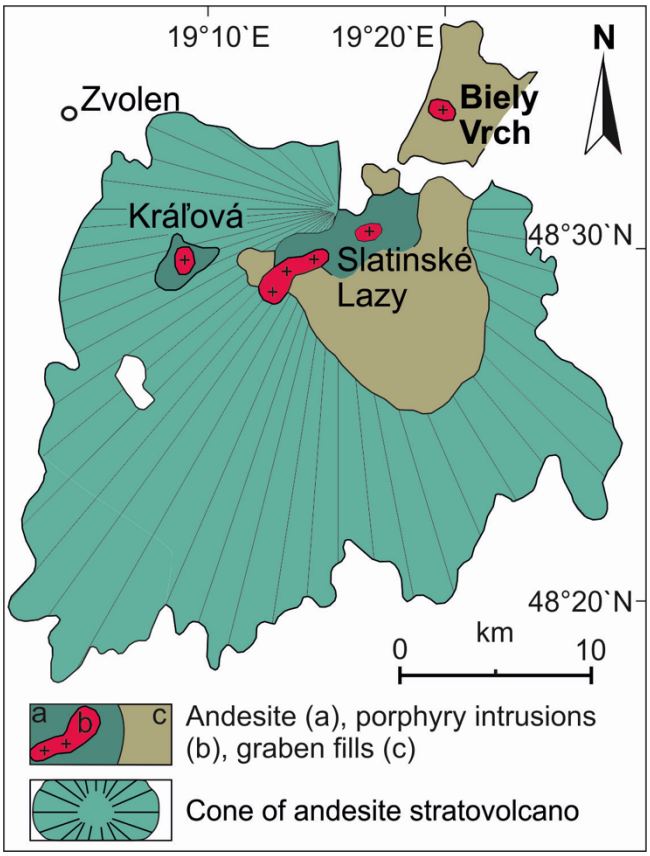

Appendix 3: The computational model and details of calculation of the hydroxyl stretching region of the vibrational spectrum of a pure γ-$Fe_2(OH)_3Cl$ (hibbingite).

Density Functional Theory (DFT) method was used to obtain information about the vibrational spectrum of a pure γ-$Fe_2(OH)_3Cl$ (hibbingite). The structural model necessary for the calculation, was derived from the isomorphic structure of $Cu_2(OH)_3Cl$, (atacamite; Wells 1994), where the structural positions of Cu atoms in the atacamite structure were substituted for Fe atoms. Then, the structure was accommodated to the published cell parameters of the hibbingite structure (Saini-Eidukat et al. 1994). The positions of hydrogen atoms were calculated to get O−H bond values of 1.1 Å in the starting structural model of hibbingite.

All DFT calculations were performed using the Vienna *Ab Initio* Simulation Package (VASP; Kressse and Hafner 1993, Kresse and Futhmüller 1996). The exchange-correlation energy was expressed in the frame of a generalized gradient approximation (GGA) using the functional proposed by Perdew et al. (1996). The Kohn-Sham equations were solved variationally in a plane-wave (PW) basis set with an energy cut-off of 500 eV in 32 *k*-points. The electron–ion interactions were described using the projector-augmented-wave (PAW) method (Blöchl 1994, Kresse and Joubert 1999). The structural relaxation was performed in two steps. First, all atomic positions were relaxed at the fixed unit cell. In the second step, the atomic positions were relaxed together with the unit cell parameters. No symmetry restrictions were applied during any relaxation procedure. The relaxation criteria were 10^{-5} eV/atom for the total energy change and 0.005 eV/ Å for the maximal allowed forces acting on each atom. To describe correctly the strong Coulomb repulsion (U) between the localized *d* electrons of Fe atom, the DFT+U approach according Dudarev et al. (1998) was applied in all calculations. The effective on-site Coulomb and exchange interaction parameters for each Fe atom were set to 4 eV and 1 eV, respectively, as used in the study of bulk goethite (Dudarev et al. 1998, Tunega 2012). The initial spin for each Fe(II) was set to 4/2 in the antiferromagnetic and also ferromagnetic state to know the preferred more stable spin

configuration. Normal vibration modes were calculated within the fixed optimized cells using a finite difference method. Normal mode analysis was performed in the frame of harmonic approximation. The Hessian was constructed from the single point energy calculations on the 6*n* structures generated from the optimized structures by displacing each of the *n* atoms in the cell in a positive and negative sense along the Cartesian directions *x, y,* and *z* (Hafner 2003). The model with high spin in the antiferromagnetic state was more stable than the ferromagnetic one (-7.6 kJ/mol). The optimised cell parameters of pure *γ*-$Fe_2(OH)_3Cl$ are *a*=6.304 Å, *b*=7.167 Å, and *c*=9.257 Å. They are in good agreement with experimentally measured data obtained from powder X-ray diffraction measurements available in the literature (Saini-Eidukat et al. 1994, Zubkova et al. 2019).

The proposed model with optimised cell parameters was used for the calculation of total vibrational bands of the pure *γ*-$Fe_2(OH)_3Cl$ (hibbingite) structure. From the calculations, the hydroxyl stretching region contained only two intense bands at 3652 cm^{-1} and 3580 cm^{-1}, representing asymmetric (IR-active) and symmetric (Raman-active) O−H stretching vibrations, respectively. Due to the harmonic approximation, the calculated values of wavenumbers are shifted to higher energies (Blöchl 1994), approximately 100 cm^{-1} for the O−H stretching modes (Balan et al. 2007). Thus, the theoretical band position of the asymmetric mode corresponds well to that published by Saini-Eidukat et al. (1994) at 3552 cm^{-1} in the IR spectrum. The theoretical peak position of the symmetric mode also corresponds to that in the Raman spectrum acquired in this work at ~3450 cm^{-1}.

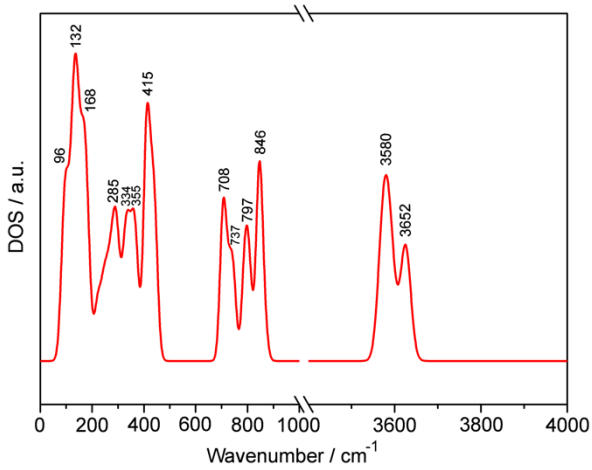

Calculated all vibrational spectrum of ideal structure of γ-$Fe_2(OH)_3Cl$.

Appendix 4: Additional EMP analyses of parahibbingite from the sample K-37-19 from the Karee mine in the Bushveld complex.

Anal.#	**1**	**2**	**3**	**4**	**5**	**6**	**7**	**8**	**9**	**10**	**11**	**12**
Fe	51.96	50.40	52.00	51.40	49.51	48.78	52.63	53.01	50.27	49.13	54.12	54.29
Mn	0.35	0.45	0.49	0.35	0.34	0.36	0.33	0.32	0.33	0.40	0.32	0.33
Mg	0.13	0.48	0.20	1.36	0.99	1.11	0.08	0.05	0.91	1.05	0.09	0.05
Si	0.24	0.65	0.35	1.54	1.71	2.74	0.03	0.03	1.67	2.61	0.03	0.03
Al	0.00	0.01	0.00	0.02	0.09	0.08	0.00	0.00	0.07	0.05	0.01	0.00
Cl	18.39	17.62	17.98	17.58	15.72	14.48	16.31	16.98	15.64	14.52	15.37	16.13
F	0.18	0.16	0.15	0.20	n.a.	n.a.	n.a.	n.a.	n.a.	n.a.	n.a.	n.a.
Na	0.03	0.21	0.07	0.12	0.00	0.00	0.04	0.02	0.01	0.00	0.05	0.02
K	0.00	0.03	0.00	0.00	0.00	0.01	0.01	0.00	0.01	0.01	0.01	0.01
Ca	0.02	0.03	0.04	0.34	0.08	0.13	0.44	0.25	0.08	0.23	0.68	0.25
Ti	0.00	0.01	0.02	0.01	0.00	0.00	0.01	0.01	0.02	0.02	0.00	0.00
Cr	0.03	0.02	0.01	0.01	0.06	0.06	0.01	0.00	0.06	0.04	0.01	0.00
Ni	0.00	0.00	0.00	0.00	n.a.	n.a.	n.a.	n.a.	n.a.	n.a.	n.a.	n.a.
Total	71.32	70.06	71.30	72.93	68.51	67.74	69.89	70.67	69.06	68.05	70.70	71.12
Normalised on the basis of 2 divalent cations (Fe+Mn+Mg+Ca)												
Fe	1.97	1.94	1.96	1.90	1.91	1.88	1.98	1.98	1.91	1.88	1.97	1.98
Mn	0.01	0.02	0.02	0.01	0.01	0.01	0.01	0.01	0.01	0.02	0.01	0.01
Mg	0.01	0.04	0.02	0.12	0.09	0.10	0.01	0.00	0.08	0.09	0.01	0.00
Si	0.02	0.05	0.03	0.11	0.13	0.21	0.00	0.00	0.13	0.20	0.00	0.00
Al	0.00	0.00	0.00	0.00	0.01	0.01	0.00	0.00	0.01	0.00	0.00	0.00
Cl	1.10	1.07	1.07	1.02	0.95	0.88	0.96	1.00	0.94	0.88	0.88	0.93
F	0.02	0.02	0.02	0.02	-	-	-	-	-	-	-	-
Na	0.00	0.02	0.01	0.01	0.00	0.00	0.00	0.00	0.00	0.00	0.00	0.00
K	0.00	0.00	0.00	0.00	0.00	0.00	0.00	0.00	0.00	0.00	0.00	0.00
Ca	0.00	0.00	0.00	0.02	0.00	0.01	0.02	0.01	0.00	0.01	0.03	0.01
Ti	0.00	0.00	0.00	0.00	0.00	0.00	0.00	0.00	0.00	0.00	0.00	0.00
Cr	0.00	0.00	0.00	0.00	0.00	0.00	0.00	0.00	0.00	0.00	0.00	0.00
Ni	0.00	0.00	0.00	0.00	-	-	-	-	-	-	-	-
OH	2.86	2.83	2.88	2.78	2.89	2.91	3.01	2.99	2.92	2.92	3.08	3.06

Appendix 5: BSE image and corresponding EMP analyses of a rare unknown phase with a composition close to Fe(OH)Cl that accompanies parahibbingite (Hib) hosted in talc (Tlc) in sample K-37-19 from the Karee mine in the Bushveld complex, South Africa. Analyses are normalised on the basis of 2 divalent cations (Fe+Mn+Mg+Ca)

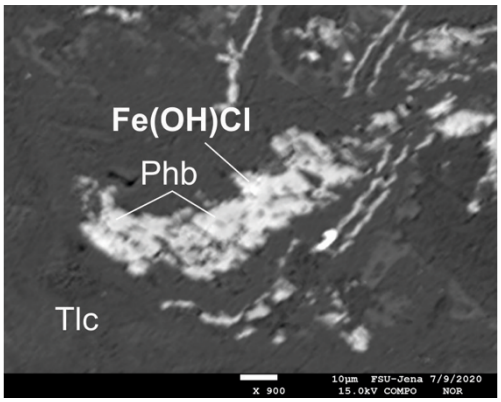

Anal.#	**1**	**2**	**3**
Fe	46.38	46.67	48.33
Mn	2.39	1.84	0.98
Mg	0.18	0.02	0.64
Si	0.08	0.04	1.07
Al	0.00	0.00	0.01
Cl	30.01	29.34	26.15
Na	0.06	0.00	0.00
K	0.01	0.01	0.01
Ca	0.12	0.23	0.04
Ti	0.01	0.01	0.40
Cr	0.03	0.00	0.03
Total	79.27	78.16	77.67
Fe	1.89	1.92	1.91
Mn	0.10	0.08	0.04
Mg	0.02	0.00	0.06
Si	0.01	0.00	0.08
Al	0.00	0.00	0.00
Cl	1.92	1.90	1.62
Na	0.01	0.00	0.00
K	0.00	0.00	0.00
Ca	0.01	0.01	0.00
Ti	0.00	0.00	0.02
Cr	0.00	0.00	0.00
OH	2.05	2.09	2.27

Appendix 6. Calculated powder X-ray diffraction data for parahibbingite, calculated for the X-ray wavelength λ = 1.54056 Å, up to 65 º2θ. Only peaks with a relative intensity of > 2 % are listed. The data were calculated with the lattice parameters from this work and the structural model for β-$Co_2(OH)_3Cl$ (de Wolff 1953).

2θ [°]	***d* spacing [Å]**	I/I_{max} **[%]**	***h k i l***
15.9	**5.55**	**42**	**-1 1 0 1**
18.3	4.83	7	0 0 0 3
19.2	4.63	7	0 1 -1 2
25.7	3.47	5	-1 2 -1 0
30.4	**2.94**	**22**	**0 2 -2 1**
31.7	**2.82**	**62**	**-1 2 -1 3**
32.2	2.78	3	2 2 0 2
38.9	**2.31**	**100**	**0 2 -2 4**
40.1	2.24	4	-2 3 -1 1
43.3	2.09	3	-2 2 0 5
46.3	1.96	4	-1 1 0 7
49.1	**1.85**	**17**	**0 3 -3 3**
51.0	1.79	5	-1 3 -2 5
52.7	**1.73**	**36**	**-2 4 -2 0**
53.7	1.71	2	0 2 -2 7
55.4	1.66	8	-1 4 -3 1
56.3	1.63	4	-2 4 -2 3
59.5	1.55	6	-2 2 0 8
60.4	**1.53**	**15**	**-2 3 -1 7**
63.1	1.47	3	0 4 -4 2

Appendix 7: EMP analyses of minerals associated with parahibbingite from sample K-37-19, taken from the Karee mine in the Bushveld complex, South Africa.

(attached Excel spreadsheet)

References cited

Balan, E., Lazzeri, M., Delattre, S., Méheut, M., Refson, K., and Winkler, B. (2007) Anharmonicity of inner-OH stretching modes in hydrous phyllosilicates: assessment from first-principles frozen- phonon calculations. Physics and Chemistry of Minerals, 34, 621–625.

Blöchl, P.E. (1994) Projector augmented-wave method. Physical Review B, 50, 17953–17979.

Cawthorn, R.G., Luvimbe, C., and Slabbert, M. (2009) Suspected presence of hibbingite in olivine pyroxenites adjacent to the UG2 chromitite, Bushveld Complex, South Africa. Canadian Mineralogist, 47, 1075–1085.

Dudarev, S.L., Botton, G.A., Savrasov, S.Y., Humphreys, C.J., and Sutton, P.A. (1998) Electronenergy-loss spectra and the structural stability of nickel oxide: an LSDA + U study. Physical Review B, 57, 1505–1509.

Hafner, J. (2003) Vibrational spectroscopy using ab initio density-functional techniques. Journal of Molecular Structure., 651-653, 3–17.

Kawohl, A., and Frimmel, H.W. (2016) Isoferroplatinum-pyrrhotite-troilite intergrowth as evidence of desulfurization in the Merensky Reef at Rustenburg (western Bushveld Complex, South Africa). Mineralogical Magazine, 80, 1041-1053.

Kresse, G., and Furthmüller, J. (1996) Efficiency of ab-initio total energy calculations for metals and semiconductors using a plane-wave basis set. Computational Materials Science, 6, 15–50.

Kresse, G., and Hafner, J. (1993) Ab initio molecular dynamics for open-shell transition metals. Physical Review B, 48, 13115–13118.

Kresse G., and Joubert J. (1999) From ultrasoft potentials to the projector augmented wave method. Physical Review, 59, 1758–1775.

Lexa, J., Štohl, J., and Konečný, V. (1999) Banská Štiavnica ore district: relationship among metallogenetic processes and the geological evolution of a stratovolcano. Mineralium Deposita, 34, 639-665.

Perdew, J.P., Burke, K., and Ernzerhof, M. (1996) Generalized gradient approximation made simple. Physical Review Letters, 77, 3865–3868.

Saini-Eidukat, B., Kucha, H., and Keppler, H. (1994) Hibbingite, γ-$Fe_2(OH)_3Cl$, a new mineral from the Duluth Complex, Minnesota, with implications for the oxidation of Fe-bearing compounds and the transport of metals. American Mineralogist, 79(5-6), 555–561.

Tunega, D. (2012) Theoretical study of properties of goethite (α-FeOOH) at ambient and high-pressure conditions. The Journal of Physical Chemistry C, 116, 6703–6713.

Wells, A.F. (1949) The crystal structure of atacamite and the crystal chemistry of cupric compounds. Acta Crystallographica, 2, 175–180.

Zubkova, N.V., Pekov, I.V., Sereda, E.V., Yapaskurt, V.O., and Pushcharovsky, D,Yu. (2019) The crystal structure of hibbingite, orthorhombic $Fe_2Cl(OH)_3$. Zeitschrift für Kristallographie - Crystalline Materials, 234, 379–382.